International Journal of Industrial Ergonomics 62 (2017) 42–47

Contents lists available at ScienceDirect

International Journal of Industrial Ergonomics

journal homepage: www.elsevier.com/locate/ergon

Effects of power tool vibration on peripheral nerve endings

Jordan Zimmerman [a, *], James Bain [b], Magnus Persson [c], Danny Riley [b]

[a] Marquette University Biomedical Engineering, United States
[b] The Medical College of Wisconsin Cell Biology, Neurobiology & Anatomy, United States
[c] Atlas Copco Tools, Sweden

ARTICLE INFO

Article history:
Received 18 February 2016
Received in revised form
16 July 2016
Accepted 18 August 2016
Available online 7 November 2016

Keywords:
Hand Arm Vibration Syndrome
Rat tail model
ISO 5349-1

ABSTRACT

Exposure to high frequency (kHz) vibration from impact power tools is overlooked in the ISO 5349-1 risk prediction for acquiring Hand Arm Vibration Syndrome. The biological effects of high frequency, power tool vibration have not been adequately studied. We characterized the magnitude and transmissibility of riveting hammer vibration in a rat tail model using a light weight piezoelectric sensor. The performance of the newly-introduced piezoelectric sensor was validated by showing its similarities to the previously published laser vibrometer. ISO 5349-1 frequency weighting revealed major risk from the 35 Hz component of the riveting hammer vibration, whereas the weighted values of the kHz components were not calculated to reach exposure action value in 24 h— However, the unweighted acceleration magnitudes at 12.4 and 16.3 kHz were about 10 and 50 times larger than the unweighted acceleration peak observed at 35 Hz. A transmissibility of <1 was calculated for 12.4 and 16.3 kHz, indicating tissue absorbance, while 35 Hz exhibited a transmissibility of 9.05, suggesting tissue resonance. The largest absolute change in acceleration was at 12.4 and 16.3 kHz, implicating that a considerable amount of high frequency vibration energy was absorbed by the tissue. A progressive reduction in intact sensory nerve endings was observed in the tissue when increasing vibration exposure from 1 min to 12 min.

© 2016 Published by Elsevier B.V.

1. Introduction

Hand-Arm Vibration Syndrome (HAVS) is a neurodegenerative and vasospastic disease observed in workers who regularly use handheld percussive, impact power tools. In the United States alone, 1.5 million workers are exposed to hand-transmitted vibration (Loffredo et al., 2009). HAVS symptoms include numbness, blanching, and tingling of the fingers as well as a loss of fine motor control (Fridén, 2001). Symptoms may be severe enough to warrant a change in occupation (Goldsmith et al., 1994).

The International Organization for Standardization (ISO) standard 5349-1 estimates the risk associated with the operation of handheld power tools in order to predict the onset of HAVS symptoms. It employs a frequency weighting calculation that places the greatest risk on vibration frequencies less than 16 Hz, and substantially less risk on vibration frequencies greater than 100 Hz (Bovenzi, 1998; Krajnak et al., 2012). The effectiveness of ISO 5349-1 is controversial, as several epidemiological studies have revealed it to both overestimate and underestimate vascular HAVS prevalence for various tool operators (reviewed in Bovenzi and Hewitt) (Bovenzi, 1998; Hewitt and Mason, 2015). There are roughly equal numbers of supporting and disagreeing studies regarding the effectiveness of the frequency weighted risk assessment described by ISO 5349-1 (Hewitt and Mason, 2015). The risk assessment may be unique to each biological effect, but is applied universally by ISO 5349-1 to all biological effects of hand-transmitted vibration, whether vascular or neurological (Hewitt and Mason, 2015).

Few studies have investigated a quantitative relationship between vibration exposure and its resulting neurological damage (Hewitt and Mason, 2015; Raju et al., 2011; Bovenzi and Ronchese, 2011). A rat tail model of hand-transmitted vibration has been developed and produces similar peripheral nerve ending damage in rats to what is observed in workers with HAVS (Loffredo et al., 2009; Raju et al., 2011). This model simulates vibration exposure experienced by bucking bar operators in conjunction with the riveting hammer. Bucking bar operators more commonly exhibit vascular HAVS symptoms (45%) than workers who operate the riveting hammer (10%), and HAVS risk for riveters is believed to be underestimated by ISO 5349-1 by a factor of 4 (McKenna et al., 1993; Dandanell and Engstrom, 1986). Exposure to a single,

* Corresponding author.
E-mail address: zimmerman.jordan@outlook.com (J. Zimmerman).

http://dx.doi.org/10.1016/j.ergon.2016.08.012
0169-8141/© 2016 Published by Elsevier B.V.

continuous, 12 min bout of bucking bar simulated vibration of the rat tail results in the destruction of lanceolate nerve endings when observed 4 days after the delivery of vibration (Raju et al., 2011). Lanceolate sensory complexes are mechanoreceptors in the dermis that encircle guard hairs and form parallel arrays of longitudinally-oriented processes of sensory nerve endings on the hair shafts (Kaidoh and Inoue, 2008; Li and Ginty, 2014). The lanceolate complexes exhibit phase-lock activity in response to sinusoidal oscillation displacements of hairs (Banks et al., 2014). Importantly, the lanceolate nerve endings are a stable population throughout the 30-day life cycle of hairs in contrast to the circular sensory nerve endings that undergo cycles of formation and regression during the hair life cycle (Johansson et al., 1997). Thus, the lanceolate complexes are amenable to the study of vibration-induced destruction of mechanoreceptor nerve endings.

The present study utilizes a rat tail vibration model to 1) introduce a low-mass, thin piezoelectric sensor that can be applied on the tail to measure vibration transmissibility and 2) assess the effect of varying vibration exposure (1,6, and 12 min) on mechanosensory peripheral nerve ending populations. The performance of the piezoelectric sensor is compared to previous measurements made by Xu et al. with the laser vibrometer (Xu et al., 2011). We predict that the destruction of lanceolate nerve endings will increase with longer periods of vibration exposure.

2. Methods

2.1. Animals

Rats were housed in AALAC-approved facilities with ad libitum access to food and water and transported to the laboratory for vibration treatment. All treatments were approved by the Medical College of Wisconsin's Institutional Animal Care and Use Committee (IACUC). Twelve female, 5-wk-old, Sprague Dawley rats were randomly assigned to one of the following four groups (n = 3/group):

(1) Control sham vibration – rats were restrained in tube cages with their tails taped to a non-vibrating platform for 12 min.
(2) 1 min vibration – animals were restrained with their tails taped to a vibrating platform for 1 min.
(3) 6 min vibration – animals were restrained with their tails taped to a vibrating platform for 6 min.
(4) 12 min vibration – animals were restrained with their tails taped to a vibrating platform for 12 min.

Upon receipt and vivarium caging of the rats, restraint-type tubes (2 in dia plastic pipes) were placed in each cage for familiarization and enrichment. The rats were acclimated to daily restraint of 12 min for 3 consecutive days prior to vibration treatment. During acclimatization, rats were loaded into the tubes, and both the restrainer and the rat's tail were taped securely to the tabletop to mimic experimental restraint conditions. Regardless of group, all rats were returned to vivarium housing for 3 days after the assigned vibration was delivered, and then euthanized.

2.2. Rat tail vibration model

The rat tail vibration model utilized a riveting hammer (Atlas Copco RRH04P, 20 psi, 40 N preload) driving a fan-shaped, steel bit platform to simulate bucking bar vibration exposure as described previously (Raju et al., 2011; Xu et al., 2011; Welcome et al., 2008). A Smart Material Corp. Macro Fiber Composite (MFC) M8503-P2 piezoelectric sensor was instrumented for recording acceleration. Shielded, flexible wires were soldered to the piezoelectric sensor and connected to a data acquisition system, comprised of a National Instruments (NI) 9222 Analog Voltage Module, a NI cDAQ-917, and LabVIEW 2013. A sampling rate of 75 kHz was chosen in order sufficiently sample the highest (16 kHz) frequency component of the vibration signal (Xu et al., 2011). For each animal, the distal end of tail vertebra C5 was positioned on top of the proximal end of the platform, as was done in previous studies using the rat tail model (Raju et al., 2011). This alignment centered vertebra C12 in the middle of the vibration platform. During vibration exposure, the sensor (113 mm × 8 mm) was positioned centrally over C12 on the dorsal tail surface and secured with masking tape (Fig. 1). In response to vibration, the ceramic within the piezoelectric sensor bends, causing the creation of an electrical potential. Data collection started when the riveting hammer began cycling, and continued throughout the entire bout of vibration. After all animals were vibrated, the sensor was taped directly onto the vibrating platform to record acceleration output from the region previously contacted by the ventral surface of the tail.

2.3. Data analysis

A Virtual Instrument (VI) was created in NI LabVIEW to record the raw voltage produced by the piezoelectric sensor and to calculate its power spectral density. Several programs were written in the C language to calculate averages and detect peaks within the previously recorded power spectral densities. C programming was more familiar to the authors, and thus preferred over LabVIEW.

Frequency weighting (ISO 5349-1) was applied to the calculated power spectrum data using Equation (1), where Mag_w is the weighted magnitude, Mag_{uw} is the unweighted magnitude, and f is the frequency of vibration. For frequencies <16 Hz, the weighted and unweighted magnitudes are identical. Ten distinct frequencies contributed nearly all of the signal's vibrational power (35, 69, 104, 139, 174, 208, 3.9 k, 8.4 k, 12.4 k, and 16.3 k Hz). The power spectrum peak for a given frequency was averaged across the entire duration of vibration. This resulted in 10 averaged power spectrum peaks, one at each of the ten dominant frequencies. The transmissibility of the rat tail was described by the quotient of the average dorsal (on the tail) and ventral (on the platform) sensor power spectrum peaks (Eq. (2)).

$$Mag_w = Mag_{uw} \times (16\ Hz/f) \tag{1}$$

$$Transmissibility = \frac{Dorsal\ Sensor\ Output}{Ventral\ Sensor\ Output} \tag{2}$$

2.4. Piezoelectric sensor sensitivity

The sensitivity (V^2 RMS/ms^{-2}) of the piezoelectric sensor was determined using two Brüel & Kjær (B&K) Vibration Exciters, Type 4809. Because the Smart Materials piezoelectric sensor is rated to record vibrations up to 3 MHz, its output was expected to be frequency dependent. The frequency response of the sensor was not provided by the manufacturer. Sensitivity was determined at each of the 10 dominant frequencies. The sensitivity test paradigm was first validated for an accelerometer (B&K Accelerometer Type 4384), resulting in an experimental sensitivity of 0.83 mV/ms^{-2} agreeing with its factory-declared sensitivity of 0.8 mV/ms^{-2}. To determine the frequency dependent sensitivities of the piezoelectric sensor, the sensor and the 4384 accelerometer were vibrated simultaneously on independent, z-axis vibration exciters. The piezoelectric sensor's output voltage was measured through the LabVIEW-based data acquisition system while the analog output

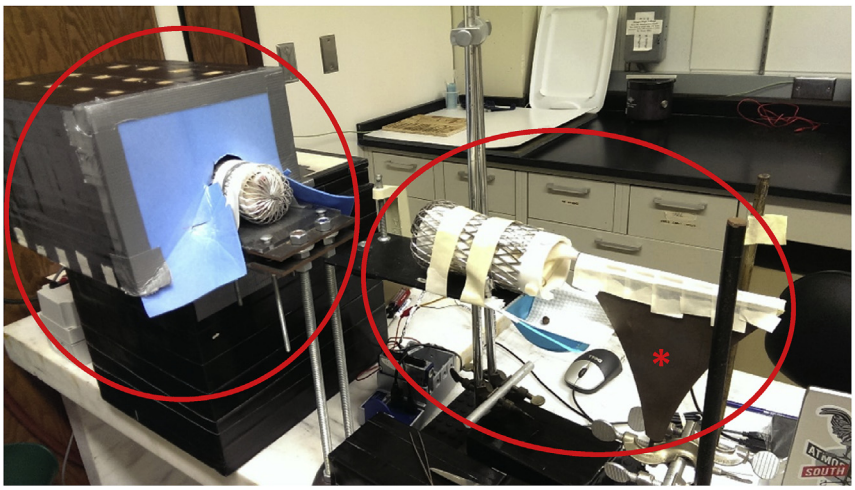

Fig. 1. A control rat (right) is restrained within the tube cage with the rat tail taped to a non-vibrating riveting hammer bit (*). The vibrated rat (left) is restrained and its tail is taped to the vibrating bit of the riveting hammer housed with the sound reduction box. During vibration, the control rat experiences restraint and noise similar to that of the vibrated rat.

acceleration was read from the 4384 accelerometer using a B&K Integrating Vibration Meter Type 2513. Three acceleration-varying trials were performed at each frequency. Sensitivities of the 3 trails were averaged, resulting in 10, frequency-dependent sensitivities. The units of the derived sensitivities (mV/ms^{-2}) were converted to V^2 RMS/ms^{-2} in order to match and convert the previously calculated power spectral density peaks.

2.5. Tail tissue fixation, sectioning, nerve staining and quantitation

A ketamine, xylazine, acepromazine-compounded anesthetic was administered intramuscularly to the left quadriceps. Non-survival surgery began when the animal no longer responded to foot-pinch. The thoracic cavity was opened to permit intracardiac perfusion fixation with phosphate buffered saline (PBS) pH 7.4 followed by 4% paraformaldehyde in PBS. After perfusion fixation, caudal tail segment C12 was excised, immersed in fixative for 2.5 h, and rinsed in PBS. Tail segments were decalcified in 10% EDTA/0.1 M Tris buffer for 10 days at 40 °C. The decalcifying solution was changed every 3 days. On day 10, the samples were rinsed 3 times (10 min each) in PBS, cryoprotected for 2 h in PBS with 20% sucrose, quick frozen in liquid nitrogen-cooled isopentane, and stored immersed in liquid nitrogen until sectioned.

For frozen sectioning, C12 tail segments were transferred into a cryostat at −20 °C, mounted and serially, cross sectioned at 60 μm. Sixteen serial sections were collected on individual drops of water and dried onto charged, Superfrost microscope slides. The dehydrated sections were ringed with rubber cement to corral the nerve immunostaining solutions. Nonspecific antibody binding was blocked with 5% normal donkey serum, 1% bovine serum albumin, and 0.3% Triton X-100/1xPBS for 20 min. Primary mouse antibody (protein gene product) PGP 9.5 (EnCor) was applied at a dilution of 1/1200 in blocking solution and incubated for 3 days at room temperature to label nerve fibers. PGP 9.5 labels central and peripheral neuronal cell bodies, axons, nerve endings, and neural support cells. Slides were rinsed 3 times (10 min each) in PBS. To demonstrate localization with fluorescence microscopy, secondary antibody, donkey anti-mouse Alexa 488-tagged was diluted in BSA/Triton and applied for 24 h at room temperature. After rinsing, the rubber cement was removed, and the sections were coverslipped with Fluoromount (Sigma) mounting medium.

Immunostained sections were examined fluorescently on a Nikon Eclipse light microscope to visualize the longitudinally-oriented nerve endings of the lanceolate complexes. To enhance visibility of the fluorescent stained nerve endings, the images were inverted in Adobe Photoshop so that the bright fluorescence was dark. The lanceolate sensory complexes enwrap hairs shafts in the dermis forming parallel longitudinal columns of lanceolate nerve endings oriented parallel to the hair (Fig. 3). Microscope images were taken of all of the lanceolate complexes in each section, and this process was repeated through the 16 serial sections. When the lanceolate complex was not completely discernible because of

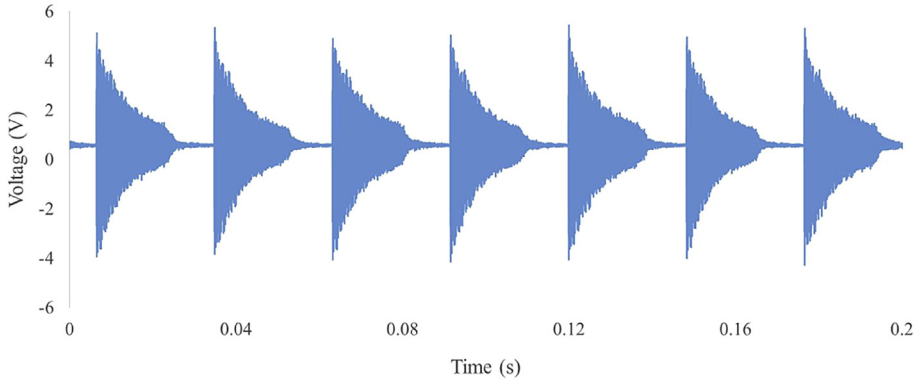

Fig. 2. Voltage signal produced by the piezoelectric sensor taped on the vibrating platform ventral to the tail.

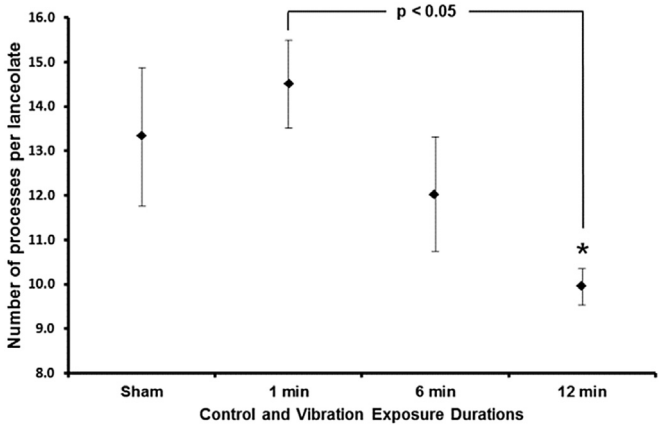

Fig. 3. Average number of lanceolate processes per lanceolate complex in tail segment C12 (mean ± sem).

plane of section orientation, the structure was not imaged. On average, similar total numbers of lanceolate complexes (94 ± 6) were taken in each of the 4 groups of rats. The number of lanceolate longitudinal endings per complex were counted in the images enlarged on a high resolution computer monitor. The average number of lanceolates per lanceolate complex was calculated and compared in the vibrated and control groups using 1-way ANOVA and post hoc Tukey statistical analysis.

3. Results

The unfiltered, magnitude-time signal of the riveting hammer recorded by the piezoelectric sensor was very similar to that recorded by the laser vibrometer in of Xu et al. (Xu et al., 2011). Both recordings were made from the bare, vibrating platform (Fig. 2).

The frequency-dependent sensitivities of the piezoelectric sensor are shown in Table 1 for the dominant frequencies. These sensitivities were used with the averaged power spectra measured by LabVIEW to calculate the unweighted and weighted RMS peak accelerations listed in Table 2. The unweighted RMS peak acceleration of the vibration signal shows dominant peaks (larger than other peaks by at least a single order of magnitude) at 12.4 and 16.3 kHz. The two dominant frequencies (12.4 and 16.3 kHz) have transmissibility values less than one; the lowest transmissibility of all 10 frequencies. The averaged, unweighted RMS peak accelerations recorded at the dorsal (on the tail) and ventral (on the platform) locations of the rat tail are provided in Table 3.

The average number of lanceolate processes per lanceolate complex after 1 and 6 min vibration exposures were not different from control, whereas lanceolate numbers are significantly ($p < 0.05$) reduced following 12 min vibration (Fig. 3). In rats vibrated 12 min, the lengths of the lanceolate processes appeared shorter and less distinct than in controls, but this additional indication of lanceolate nerve ending degeneration proved too difficult to quantify (Fig. 4). The supportive Schwann cells surrounding the lanceolate complex normally stain very lightly for PGP9.5 immunoreactivity compared to nerve fibers. However, following 12 min vibration they were stained darker (Fig. 4). The increased PGP9.5 staining is consistent with Schwann cell phagocytosis of vibration-disrupted lanceolate nerve endings containing PGP9.5 protein.

4. Discussion

The similarity in appearance of the time domain vibration signals recorded by the piezoelectric sensor and the laser vibrometer suggests that the MFC piezoelectric sensor was successful in measuring power tool vibration in the rat tail model (Xu et al., 2011). Using the experimentally-derived sensitivities, the RMS peak accelerations are also comparable to those collected by the laser vibrometer (Xu et al., 2011). The unweighted RMS acceleration

Table 1
Sensitivities of the piezoelectric sensor for each of the 10 dominant frequencies observed in the riveting hammer signal. Sensor produces the least voltage (therefore, is the least sensitive) at 16.3 kHz.

Frequency (Hz)	Sensitivity (V^2 RMS/ms^{-2})	Stdev (V^2 RMS/ms^{-2})	Coefficient of variation
35	1.031E-04	3.051E-05	0.296
69	2.148E-04	6.188E-05	0.288
104	2.708E-04	1.340E-04	0.495
139	3.007E-04	1.723E-04	0.573
174	3.028E-04	2.093E-04	0.691
208	3.314E-04	2.010E-04	0.607
3908	8.375E-03	1.182E-02	1.412
8394	2.497E-03	3.244E-03	1.299
12 436	2.590E-05	2.367E-06	0.091
16314	1.135E-05	4.132E-06	0.364

Table 2
Using the derived sensitivities form Table 1, the measured power spectra density peaks are converted into unweighted, peak RMS accelerations for each frequency. Equation (1) is used to calculate the weighted peak RMS accelerations.

Frequency (Hz)	Average power spectra density magnitude (V^2 RMS)	Unweighted peak RMS acceleration (ms^{-2})	Weighted peak RMS acceleration (ms^{-2})
35	0.0014	19.6021	8.9776
69	0.0008	5.0077	1.1540
104	0.0004	2.3438	0.3600
139	0.0001	0.4753	0.0547
174	1.7992E-05	0.0840	0.0077
208	3.3897E-05	0.1447	0.0111
3908	6.5053E-05	0.0110	4.4967E-05
8394	2.4537E-06	0.00139	2.6489E-06
12 436	0.0037	203.7341	0.2621
16314	0.0078	966.8531	0.9483

Table 3
Unweighted dorsal and ventral accelerations are used with Equation (2) in order to calculate the transmissibility of the rat tail.

Frequency (Hz)	Unweighted ventral peak RMS acceleration (ms^{-2})	Unweighted dorsal peak RMS acceleration (ms^{-2})	Transmissibility
35	19.6021	177.3992	9.05
69	5.0077	45.5703	9.10
104	2.3438	20.7189	8.84
139	0.4753	1.4069	2.96
174	0.0840	0.1453	1.73
208	0.1447	0.6871	4.75
3908	0.0110	0.1168	10.63
8394	0.0014	0.0005	0.37
12436	203.7341	75.3816	0.37
16314	966.8531	270.7189	0.28

of the vibrating platform at the operational frequency (35 Hz) is measured to be 20 ms^{-2} by both devices (Xu et al., 2011). The laser vibrometer RMS accelerations remain around 20 ms^{-2} for the subsequent harmonics until 500 Hz, while the piezoelectric sensor shows a sharp decline in the magnitude of subsequent harmonics following the operational frequency (Xu et al., 2011). Xu et al. found a peak of about 2000 ms^{-2} at 16 kHz while we measured a peak of about 1000 ms^{-2} at 16 kHz (Table 2) (Xu et al., 2011). There are several possible reasons for this difference in magnitude. In terms of size, the piezoelectric sensor is 113 mm in length, and therefore measures vibration along multiple vertebra, whereas the laser vibrometer measures from a length spanning only a few millimeters and measures acceleration at a single vertebra (Welcome et al., 2008). In addition, the acceleration magnitudes of the B&K exciters used to derive the sensitivity of the piezoelectric sensor at 16 kHz were at least 10 fold lower than the acceleration measured by the laser vibrometer. The large variation of sensitivities implies that the sensitivity of the piezoelectric sensor is dependent on the magnitude of acceleration. The acceleration measured by the piezoelectric sensor at 35 Hz is believed to be closer to the acceleration measured by Xu et al. because the calibration acceleration magnitudes range from 43 to 80 ms^{-2}, and the B&K accelerometer operated within its bandwidth. Simultaneous acceleration measurements from the laser vibrometer and piezoelectric sensor are necessary for a more precise calibration.

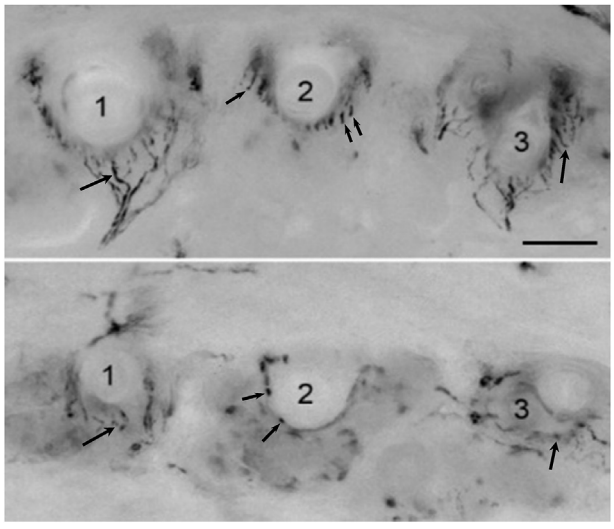

Fig. 4. Inverted fluorescence images of rat tail segment C12 stained with PGP9.5 for nerve fibers. Lanceolate complexes encircle hairs 1, 2 and 3 in a control (upper panel). The parallel longitudinal lanceolate nerve processes (arrows) are more numerous, regularly spaced and longer than those in the 12 min vibrated rat (lower). The reduction in lanceolate sensory nerves indicates vibration-induced destruction. Bar in upper panel equals 63 μm.

The 12.4 kHz peak measured by the piezoelectric sensor was not observed by the laser vibrometer (Xu et al., 2011). Identical model riveting hammers were used in our studies, so it is unlikely that the dominant 12.4 kHz component is due to the riveting hammer. The 12.4 kHz peak may be the resonant frequency of the piezoelectric sensor when attached to the fan-shaped bit, vibrating platform. Both studies enclosed the platform in a noise reduction box. Our study used a heavy metal walled box whereas Xu et al. used a set of nested Styrofoam boxes. The reflection of 12.4 kHz vibrations within the noise attenuation box may contribute to its dominate presence in the power spectrum. Further side by side characterization of the piezoelectric sensor with the laser vibrometer is necessary to verify the sensor's utility for power tool vibration measurement. The present study demonstrates that the piezoelectric sensor is a valid means of measuring accelerations of the rat tail.

For the rat tail model, the largest absolute changes in unweighted acceleration at the dorsal and ventral locations are observed at 16 kHz in both this study and Xu et al. (Table 3) (Xu et al., 2011). The high frequency (kHz) vibrations of the riveting hammer uniquely exhibit shock wave energy, which is thought to reflect from deep tissues into the superficial layers, thus damaging cutaneous peripheral nerve endings (Raju et al., 2011). Bucking bar operators more commonly exhibit HAVS symptoms as oppose to riveters, and are exposed to larger amounts of kHz frequency vibration (McKenna et al., 1993; Dandanell and Engstrom, 1986). These factors suggest that the 16.3 kHz component induces harmful pathological consequences. Low frequencies exhibit transmissibility values greater than 1, indicating resonance of the tail, and may have contributed to the observed nerve damage. The larger, absolute changes in unweighted acceleration at 16.3 kHz (696 ms^{-2}) compared to 35 Hz (158 ms^{-2}) further suggests the need to consider kHz vibration risk. If using frequency weighted accelerations, hand-arm vibration risk is only associated to the 35 Hz component of the vibration signal. A measured, weighted acceleration of almost 9 ms^{-2} requires 37 min of vibration exposure to reach the exposure action value (EAV) and 159 min of exposure to reach the exposure limit value (ELV).

Increasing the duration of vibration exposure from 1 to 12 min diminished the average number of PGP9.5 stained lanceolate processes per complex, suggesting longer exposure to vibration increases the destruction of lanceolate nerve processes (Figs. 3 and 4). While PGP9.5 detects enzymes involved in both regeneration and degeneration of peripheral nerve endings, the unorganized appearance of the lanceolate nerve endings after 3 days of rest suggests degeneration. Degeneration of lanceolate nerve endings is believed to decrease mechanosensitivity, a prevalent symptom of HAVS. The mechanosensitivity of rat tails post vibration has not been studied, and needs to be further investigated in order to suggest its correlation to lanceolate ending degeneration. We have previously reported a reduction in noxious heat response time in

rat tails which received 12 min of riveting hammer vibration (Raju et al., 2011). This suggests that thermoreceptors and/or nociceptors in the vibrated rat tail are damaged in response to vibration. The lanceolate nerve endings in the rat tail exist solely in hair follicles, which are not present in the palm of the human hand and fingers. Further studies are needed to investigate the neurological response to power tool vibration of mechanosensory structures directly in contact with the power tool itself.

5. Conclusion

The MFC M8503-P2 piezoelectric sensor and associated NI hardware/software are validated for measuring time and frequency domain accelerations of the riveting hammer rat tail model. Simultaneous measurements with the sensor and laser vibrometer are needed to further quantitatively characterize the sensor's voltage response to vibration. The present study determined that the lanceolate nerve complexes in the rat tail are appropriate for demonstrating reduction in lanceolate nerve endings, which is likely to disrupt their mechanoreceptive function. The degree of nerve ending loss increased with the duration of vibration exposure. Future studies are necessary to characterize the effects of multiple days of exposure to simulate tool patterns of the workplace and to determine whether repeated vibration of nerve endings destroys sensory neurons and their ability to restore mechanosensitivity.

Acknowledgements

The author would like to thank the Wisconsin Space Grant Consortium for financially supporting the completion of this research.

References

Banks, R.W., Cahusac, P.M.B., Graca, A., et al., 2014. The Journal of Physiology Glutamatergic Modulation of Synaptic-like Vesicle Recycling in Mechanosensory Lanceolate Nerve Terminals of Mammalian Hair Follicles, 10, pp. 2523–2540. http://dx.doi.org/10.1113/jphysiol.2012.243659, 2013.

Bovenzi, M., 1998. Exposure-response relationship in the hand-arm vibration syndrome: an overview of current epidemiology research. Int. Arch. Occup. Env. Heal 71, 509–519.

Bovenzi, M., Ronchese, F., 2011. A Longitudinal Study of Peripheral Sensory Function in Vibration-exposed Workers, pp. 325–334. http://dx.doi.org/10.1007/s00420-010-0549-8.

Dandanell, R., Engstrom, K., 1986. Vibration from riveting tools in the frequency range 6 Hz-10 MHz and Raynaud's phenomenon. Scand. J. Work Environ. Heal 12 (4), 338–342. http://dx.doi.org/10.5271/sjweh.2133.

Fridén, J., 2001. Vibration damage to the hand: clinical presentation, prognosis and length and severity of vibration required. J. Hand Surg. Br. Eur. Vol. 26 (5), 471–474. http://dx.doi.org/10.1054/jhsb.2001.0633.

Goldsmith, P.C., Molina, F.A., Bunker, C.B., et al., 1994. Cutaneous nerve fibre depletion in vibration white finger. J. R. Soc. Med. 87 (July), 377–381.

Hewitt, S., Mason, H., 2015. A critical review of evidence related to hand-arm vibration syndrome and the extend of exposure to vibration. Derbys. Engl. pgs. 7, 12, 21, 23, 25, 26, 39.

Johansson, O., Botchkarev, V.A., Eichmu, S., 1997. Hair Cycle-Dependent Plasticity Skin Hair Follicle Inn. 395 (April), 379–395.

Kaidoh, T., Inoue, T., 2008. N-Cadherin Expression in Palisade Nerve Endings of Rat Vellus Hairs, 534, pp. 525–534. http://dx.doi.org/10.1002/cne. May 2007.

Krajnak, K., Riley, D.A., Wu, J., et al., 2012. Frequency-dependent effects of vibration on physiological systems: experiments with animals and other human surrogates. Ind. Health 50, 343–353. http://dx.doi.org/10.2486/indhealth.MS1378.

Li, L., Ginty, D.D., 2014. The structure and organization of lanceolate mechanosensory complexes at mouse hair follicles. Elife 2014 (3), 1–24. http://dx.doi.org/10.7554/eLife.01901.001.

Loffredo, M.A., Yan, J.G., Kao, D., Lin, L.Z., Matloub, H.S., Riley, D.A., 2009. Persistent reduction of conduction velocity and myelinated axon damage in vibrated rat tail nerves. Muscle Nerve 39 (6), 770–775. http://dx.doi.org/10.1002/mus.21235.

McKenna, K.M., McGrann, S., Blann, A.D., Allen, J.A., 1993. An investigation into the acute vascular effects of riveting. Br. J. Ind. Med. 50 (2), 160–166. http://dx.doi.org/10.1136/oem.50.2.160.

Raju, S.G., Rogness, O., Persson, M., Bain, J., Riley, D.A., 2011. Vibration from a riveting hammer causes severe nerve damage in the rat tail model. Muscle Nerve 44 (November), 795–804. http://dx.doi.org/10.1002/mus.22206.

Welcome, D.E., Krajnak, K., Kashon, M.L., Dong, R.G., 2008. An investigation on the biodynamic foundation of a rat tail vibration model. Proc. Inst. Mech. Eng. H. 222, 1127–1141. http://dx.doi.org/10.1243/09544119JEIM419.

Xu, X.S., Riley, D.A., Persson, M., et al., 2011. Evaluation of anti-vibration effectiveness of glove materials using an animal model. Biomed. Mater Eng. 21, 193–211. http://dx.doi.org/10.3233/BME-2011-0669.